Force sensing resistors used as plantar impedance plethysmography electrodes

Isabel Morales*, Rafael González-Landaeta†, and Franco Simini*
*Núcleo de Ingeniería Biomédica, Universidad de la República, Hospital de Clínicas, p. 15 sala 2, Av. Italia S/N, 11600 Montevideo, Uruguay
†Ingeniería Eléctrica y Computación, Universidad Autónoma de Ciudad Juárez, Av. del Charro 450 nte., 32310 Ciudad Juárez, Chihuaha, México

***Abstract*—Diabetic Foot Ulcers are an ominous consequence of Diabetic Foot. To develop a multidimensional lesion warning device, several variables must be considered, among which vascular parameters. To minimize the number of sensors, we investigate the use of standard flexible Force Sensing Resistors, FSR402 and FSR406, to detect not only plantar pressure, but also bioimpedance plethysmography. Since FSRs include conductive electrodes covered by polymer film, the interface with the subject can be considered a capacitive electrode. We present a special impedance plethysmography circuit to inject current using FSRs and measuring the resulting voltage from other FSRs contacts. Impedance plethysmography simulations with two modelled FSRs, two contacts each, was not successful but using four FSRs, one capacitive contact each, shows a precision within 4% of the expected FSR resistor value. Impedance plethysmography system was verified with simultaneously matching ECG-lead I, Ag-AgCl and capacitive electrodes signals alongside power spectra. For the first time, four sole pressure sensors are used also as bioimpedance electrodes to detect cardiac activity with standard components at frequencies up to 50 kHz, simulated as well as experimentally verified on one healthy subject.**

***Index Terms*—Diabetic foot ulcer, force sensing resistor, bioimpedance, impedance plethysmography, plantar electrodes, wearable device.**

I. Introduction

DIABETES MELLITUS (DM) is a growing public health concern worldwide [1] and one of its several complex complications is diabetic foot. In most cases persons with DM have similar induced problems such as sustained hyperglycaemia, diabetic peripheral neuropathy and peripheral artery disease. Indeed, the process that leads to a diabetic foot ulcer (DFU) is a consequence of two or more of these risk factors present for a given person [2].

The identification of the at-risk foot and regular foot examination include such objective and subjective information as plantar pressure distribution, vibration perception and vascular status. The follow-up consists, in case no lesions are apparent yet, mostly of footwear solutions and pressure offloading [3]. Once the DFU is diagnosed, thermography, plantar pressure and temperature measurements are used to monitor it from a medical visit to the next one. This is the case when all prevention fails since the DFU is now manifest.

In an attempt to anticipate and understand DFUs, a number of technologies have been used in the outpatient office to evaluate the imminence of lesions. Thermography can provide real-time physiological imaging to help identify a small rise in temperature which is considered an early sign of DFU [4]. In thermography, the emitted energy from a living tissue is usually interpreted as a color-coded image. It allows to estimate the temperature distribution of an area, regardless of its shape. This evaluation can only be performed on the naked foot in the physician's office. The skin temperature distribution with its pressure related pattern are being jointly studied [5]. From a pressure ulcer prevention research perspective, the temperature distribution may be linked to soft tissue deformation. Kottner states that if the temperature and humidity around the foot is preserved, no pressure ulcer should develop [6].

Pressure sensors continuously measure plantar pressure and could provide a valuable feedback to the diabetic patient [3]. Current research focuses on the determination of pressure thresholds to predict high DFU risk [7]. This risk is assessed during a medical visit independently of the dynamic functional components of gait [8]. Plantar pressure can be measured by footprint infrared imaging scan, force plate, or pressure insoles. Nowadays, several baropodometric systems, to be used in clinical settings, are commercially available [9] [10] [11].

High plantar pressure increases the risk of developing DFUs and managing its peak pressure is therefore important. But the assessment of the at-risk foot never involves plantar pressure by itself because of its poor specificity [12].

To monitor diabetic foot health and to provide a better control over any imminent foot lesion, a review of the literature suggests a clear demand of an early alert device. We have thus defined, as a possible solution, an inexpensive wearable device, named DIAPODAL. Our goal is to alert in time the person so as to keep ulcer risk at a low level. This would be accomplished by continuous assessment of skin parameters such as temperature, humidity, pressure, friction and vascular status by means of bioimpedance plethysmography. By combining these parameters a comprehensive pre-ulcer score could be defined.

Bioimpedance is capable of long-term monitoring of skin integrity [13]. Furthermore, an appropriate selection of measurement frequencies can unveil characteristics of different skin layers, tissue depths and vascular status. However, there are no studies showing bioimpedance as a real time DFU prevention tool. Impedance plethysmography (IPG) is a technique to detect variations in electrical impedance related to changes in volume such as the vascular sector or other body parts. A tetra-polar bioimpedance measurement can detect volume changes due to blood flow [14] powered by the heart [15].

This paper aims to study the feasibility of using standard force sensors as plantar bioimpedance electrodes.This intermediate requirement during the design of the new DIAPODAL device stems from the necessity to reduce as much as possible the number of sensors in the diabetic person's shoe. To validate such use, we use force sensing resistors as bioimpedance electrodes to obtain an IPG signal. If the set-up performs correctly as an impedance plethysmograph to monitor heart rate, then the sensor will have performed correctly as a bioimpedance electrode.

The present article is an extension of the results presented in MeMeA 2021 [16] in that it includes a step further in the feasibility analysis to reduce the number of sensors necessary to describe the multidimensional state of the foot during gait.

II. Force sensors used as electrodes

A. Force sensor resistor modelling

A Force Sensing Resistor (FSR) consists of a resistance which varies with the pressure applied on it. It can be used to monitor specific plantar pressure points. Standard FSR sensors are passive devices made of polymers. Their force sensitivity range is a good option for pressure signal acquisition. There are several models, fabricated in various sizes, all of which have two solder extremities stapled through the flexible substrate to contact the semi-conductive material [17]. Table I shows the specificity of FSR402 and FSR406.

TABLE I: Force Sensing Resistors Specifications

Feature	FSR402	FSR406	Units
Actuation Force	0.10	0.10	N
Force measuring range	0.10 - 10.0	0.10 - 10.0	Kg
Size	18.28 (diameter)	43.69 x 43.69	mm
Thickness	0.20	0.20	mm
Stand-off resistance	>10M	>10M	Ω

Fig.1 shows the exploded views and the proposed schematic of the four layers of a FSR402 and FSR406 models. This exploded view helps understand the use of a FSRs as a capacitive electrode. First and third layers work as insulators, second layer as top substrate with printed carbon based ink and the fourth layer as a conductive bottom substrate with its conductive printed pattern

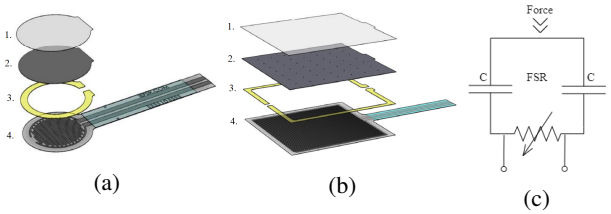

(a) (b) (c)

Fig. 1: Pressure force sensor resistor exploded view: (a) FSR402 (b) FSR406 and (c) plantar view proposed schematic [16]. Adapted from commercial material by [17].

Bioimpedance applications use different types of electrodes: i) Ag-AgCl, ii) contact or dry electrodes and iii) capacitive electrodes. Being in contact with the skin, a FSR could also be used simultaneously for yet other functions such as bioimpedance. Due to its constructive elements, each FSR could perform as a conventional capacitive electrode.

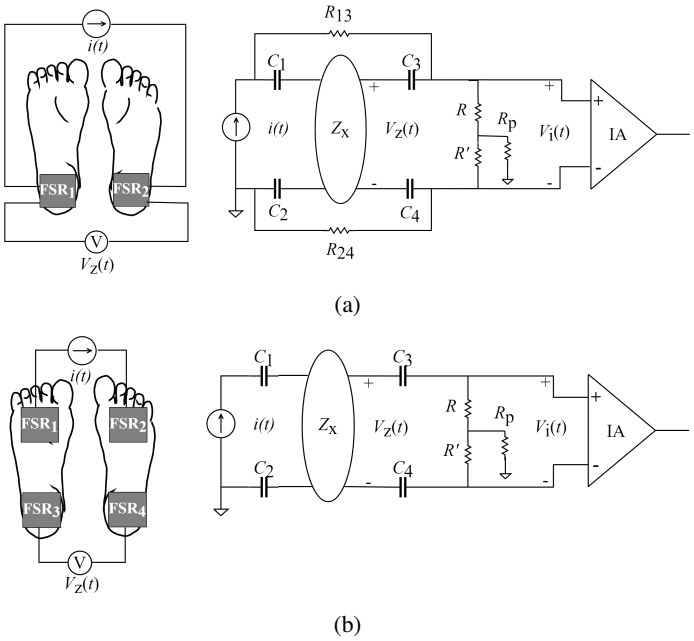

Fig. 2: Feet connection set-up and equivalent bioimpedance measurement circuits: (a) two plantar force sensor resistors and (b) four plantar force sensor resistors.

The FSR is usually modelled as a resistance in parallel with a single capacitance which is assumed to be the unique capacitance of the entire sensor [18]. In contrast, we have modelled FSRs [16], as show in Fig. 1c, with two capacitors interconnected by a force-dependent resistor. This resistor has two embedded wire leads which can be assumed to have two coupling capacitors with the underlying foot both terminated by a polymer surface which acts as a capacitor with the skin as the second electrode. This arrangement follows the configurations of Fig. 2, a complete tetra-polar bioimpedance measurement circuit as described by Bertemes-Filho et al. [19]: Let Z_X be the foot impedance.

In case the bioimpedance measurement is attempted using only two FSRs (Fig. 2a), we found an unstable and unpredictable situation because of the unknown bypassing currents through R_{13} and R_{24}. To overcome this, we have used four FSRs (Fig. 2b.)

B. Two plantar force sensors

The set-up of Fig. 2a uses two FSRs, with four capacitive contacts with the foot, C_1=C_2=C_3=C_4=C, each pair of capacitors is bypassed by a force-dependent resistor, either R_{13} or R_{24}.

Let $V_i(\omega)$ be the input voltage to the instrumentation amplifier (IA) in Fig. 2a. We can calculate $V_i(\omega)$ from the tetra-polar bioimpedance circuit parameters $V_Z(\omega)$ and $i(\omega)$.

In order to estimate $V_i(\omega)$ as a function of $V_Z(\omega)$, consider Fig. 3 where R_i and C_i represent the common-mode input impedance Z_i of the IA. Let $V_A(\omega)$ be the voltage at one of the nodes of the Voltage Controlled Current Source (VCCS). Fig.

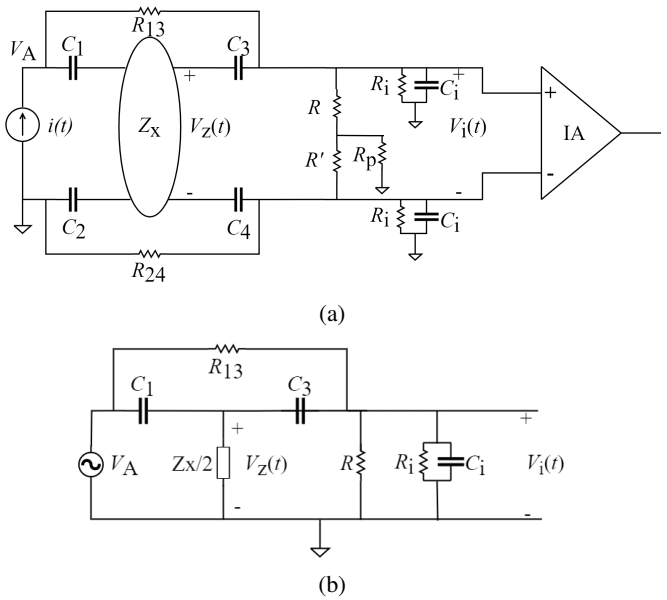

Fig. 3: Bioimpedance measurement circuits using two force sensor resistors. (a) Full circuit (b) Equivalent semi circuit.

3b shows one half of the circuit which, applying Kirchhoff's current law to two nodes, results in equation 1 and equation 2:

$$\frac{V_Z(\omega) - V_i(\omega)}{X_C} + \frac{V_Z(\omega) - V_A(\omega)}{X_C} + \frac{V_Z(\omega)}{Z_X} = 0 \quad (1)$$

$$\frac{V_i(\omega) - V_Z(\omega)}{X_C} + \frac{V_i(\omega) - V_A(\omega)}{R} + \frac{V_Z(\omega)}{Z_i} = 0 \quad (2)$$

Combining (1) and (2), the solution is:

$$V_i(\omega) = V_Z(\omega)\frac{2 + 2\frac{X_C}{Z_X} + \frac{R}{X_C}}{2 + \frac{R}{(X_C||Z_i)}} \quad (3)$$

Assuming $Z_i \approx X_{Ci}$, equation 3 can be rewritten as:

$$V_i(\omega) = V_Z(\omega)\frac{2 + \frac{2}{j\omega C Z_X} + j\omega RC}{2 + j\omega R(C_i + C)} \quad (4)$$

And considering $C_i << C$, equation 4 becomes:

$$V_i(\omega) \approx V_Z(\omega)\frac{2 + \frac{2}{j\omega C Z_X} + j\omega RC}{2 + j\omega RC} \quad (5)$$

In the frequency range we use, equation 5 can be simplified:

$$V_i(\omega) \approx V_Z(\omega)\frac{2 + \frac{2}{j\omega C Z_X}}{2} = I_Z(\omega) Z_X \frac{1}{j\omega C Z_X} \quad (6)$$

where $I_Z(\omega)$ is the current flowing through Z_X:

$$I_Z(\omega) = I\frac{R_{13} + \frac{2}{j\omega(C_3 + C_i)}}{R_{13} + \frac{1}{j\omega C_1} + \frac{1}{j\omega(C_3 + C_i)}} \quad (7)$$

From equation (7), it can be seen that the current that flows through Z_X not only depends on the frequency, but also on the bypass resistance R_{13} (or R_{24}). In the extreme case $R_{13} \to \infty$ (an open circuit) $I_Z(\omega) = I$ which does not depend on the frequency. For all other values of the bypass resistance, the current $I_Z(\omega)$ is diminished. Therefore, the presence of R_{13} and R_{24} is a problem for bioimpedance measurement accuracy because only a fraction of the current flows through the tissues and is detected as resulting voltage.

At 10 kHz, with unloaded FSRs, R_{13} y R_{24} were almost open circuits. At the same 10 kHz when the subject was standing on the FSRs, the reactance of C_1 and C_2 was much higher than the resistances R_{13} and R_{24} which caused a lower current to flow through Z_X. The remanent current (through R_{13} and R_{24}) may saturate the IA because of the very high input impedance. At much higher frequencies (100 kHz e.g.) a great share of the injected current flows through Z_X. Thus, resulting in smaller currents to the IA input. Equation (7) summarizes this behavior which can be checked assigning to ω respectively $\omega = 0$ and $\omega \to \infty$.

C. Four plantar force sensors

The set-up of Fig. 2b uses four FSRs, two under the heels and two under the metatarsal bones. The metatarsal pair of FSRs is used to inject a low-intensity and high-frequency current, while the heel pair is connected to the voltage meter. This configuration with capactive contacts is similar to that presented by Luna and Pallàs-Areny [20].

The configuration of Fig. 4a has no bypass resistor because four FSRs are used to detect the IPG. The circuit analysis is here much simpler [20]. In Fig. 4b, solving $V_i(\omega)$ as a function of $V_z(\omega)$, with $C_3 = C$ and $Z_i = R_i||X_{ci}$, results in:

$$V_i(\omega) = V_z(\omega)\frac{(R + R_p)||Z_i}{X_C + (R + R_p)||Z_i} \quad (8)$$

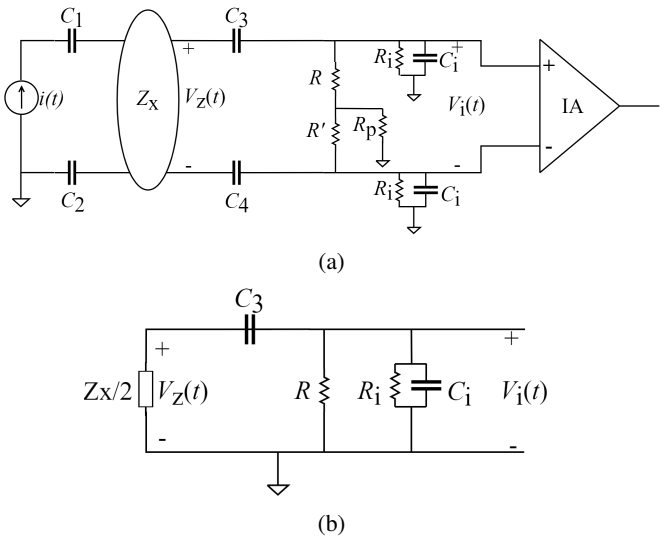

Fig. 4: Bioimpedance measurement circuits using four force sensor resistors. (a) Full circuit (b) Equivalent semi circuit.

Considering $Z_i \approx X_{Ci}$ and $X_{Ci} << R$, equation (8) can be rewritten as:

$$V_i(\omega) \approx V_z(\omega)\frac{\frac{1}{j\omega C_i}}{\frac{1}{j\omega C+\frac{1}{j\omega C_i}}} = V_z(\omega)\frac{C}{C+C_i} \tag{9}$$

Where the IA input, $V_i(\omega)$, is the result of a voltage divider as shown in Fig. 4b.

III. Materials and Methods

A. Plantar force sensing resistors

We have done previous work on foot pressure sensing using several FSR402s model under the sole. Our 24-sensor insole design [21] gave accurate results grouped in 10 anatomical areas for clinical analysis, both static and dynamic, showing 16 frames per second plantar color coded images. As the force increased, the resistance of the sensors decreased. The derived knowledge led us to formulate the present hypothesis that these sensors can have a double use: both as pressure sensors and bioimpedance electrodes.

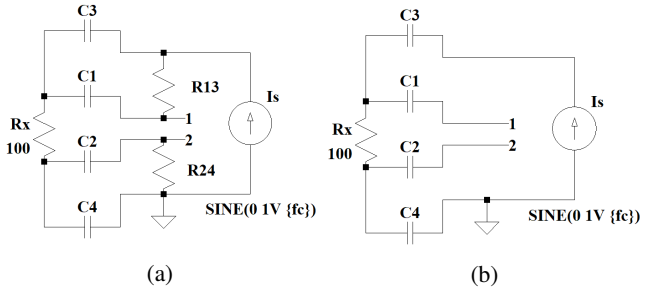

Fig. 5: Four capacitor model simulation schematic: (a) loaded FSRs show R_{13} and R_{24} bypassing resistors and (b) unloaded FSRs have high resistances allowing the tetra-polar circuit to accurately sense R_x differences during the IPG cycle.

B. Simulations

We used LTspice software from Analog Devices [22]. For simulation purposes, let R_x be the tissue resistance seen by the foot electrodes.

1) First simulation: The simulation schematic of Fig. 5a was used to vary the resistance R_x in steps of 50 Ω from 100 Ω to 200 Ω. Injected current was simulated as 1 mA at sinusoidal frequency carrier f_c of 10 kHz, 500 kHz and 1 MHz. Capacitance was arbitrarily set at 1 nF for both capacitors, C_1 and C_3 for FSR_1 and C_2 and C_4 for FSR_2 [16].

2) Variable capacitance simulations: Simulation was done for both circuits of Fig. 5 where the R_x value was estimated using the expression V_{12}/I_s. Simulation of Fig. 5a (2 FSRs) and Fig. 5b (4 FSRs) were performed. For each case, f_c was adjusted to 10 kHz, 50 kHz, 100 kHz, 500 kHz, 1 MHz. The capacitance values of 30 pF and 173 pF used were measured previously for FSR402 and FSR406 respectively.

C. Experimental impedance plethysmography set-up

The measurement system of Fig. 6 includes a four-electrode IPG configuration and comprises the VCCS adjusted to a given frequency carrier, fc. The VCCS has been implemented using the configuration presented in [23] (without DC Feedback) using a Current-Feedback Amplifier (CFA) AD844 [24]. In order to block any dc current, a blocking capacitor of 1 uF was added in series with the VCCS ouput (not shown in Fig. 6). The sinusoidal signal was obtained from an arbitrary waveform generator 33522A (Keysight). The front-end is an AC coupled amplifier to acquire the differential amplitude-modulated (AM) signal. An INA111 [25] was used as the Instrumentation Amplifier (IA), which has a common input impedance of 1 GΩ shunted by 3 pF. The AM signal is demodulated by a synchronous demodulator implemented by a switched-gain amplifier [26], where the AM signal is multiplied by a reference square waveform, $r(t)$, obtained from the TTL output of the arbitrary waveform generator. The analog switch used in the demodulator is the ADG436 [27], which has an $R_{ON} = 20\ \Omega$. Finally, the demodulated signal is amplified by a factor of $10\text{x}10^3$ and filtered to reduce the contribution of electromagnetic interference and electronic noise. For this, two first order passive band-pass filters have been implemented, one at the output of the synchronous demodulator and the other at the output of the entire system.

A healthy person (one of the authors) agreed to be connected to the IPG system. The IPG signals of the subject standing still were in most trials simultaneously measured with a standard ECG, lead I, during 10s. The signals were acquired at 200 Hz using a DSOX2014A oscilloscope from Keysight. The IPG signals are then FIR band-pass filtered (0.3 Hz - 4 Hz) for power spectrum analysis. For signal processing a Python script with SciPy ecosystem [28] was implemented.

1) Impedance plethysmography with Ag-AgCl electrodes: In order to test the performance of the system shown in Fig.6, four Ag-AgCl disposable electrodes have been used. In each leg, two ECG electrodes were placed externally, one

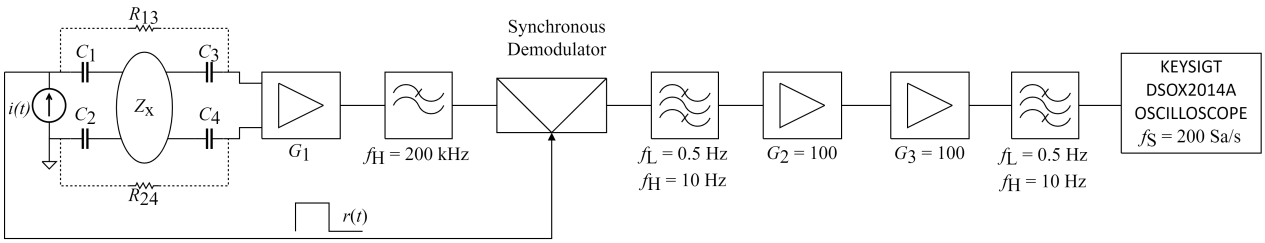

Fig. 6: Impedance plethysmography foot bioimpedance block diagram: The gain G_1 is on the order of 10, depending upon the equivalent bioimpedance measurement circuit of Fig. 2.

proximal and one distal with respect to the malleolus. So the contribution of the IPG signal refers to the same limb as that obtained using plantar electrodes. To measure V_i, an AC-coupled front-end suppresses the contribution of mains interference and $1/f$ noise from the IA [29].

2) Impedance plethysmography with aluminum pads: aluminum (Al) square pads (2 cm x 2 cm) were used as capacitive electrodes, soldered to 1 mm^2 section insulated wires. Two electrodes were located under each heel of a healthy subject. The same materials, circuits, and configuration of Fig. 2a and Fig. 6 have been used and electrodes were located between the shoe sole and the barefoot.

3) Impedance plethysmography with force sensors: To ascertain the possibility to use the parts of an FSR as a bioimpedance electrode, two impedance plethysmograph approaches as described in Fig. 2 were tested using the measurement system of Fig. 6. In both cases, the FSR406 was used. Contact capacitance was measured with handheld LCR U1733C oscilloscope from Keysight, obtaining $C_{FSR} = 173$ pF. Resistance R_{FSR} of less than 100 Ω was measured in a subject of 85 kg (one of the authors) standing on the FSR. The carrier frequency f_c was adjusted to 10 kHz, 50 kHz and 100 kHz. The voltage divider of Fig. 4a and the gain G_1 of Fig. 6 were adjusted to avoid saturation of the IA.

IV. Results

A. Simulations

1) First simulation: Fig. 7 shows that at 10 kHz there is no significant change with R_x in voltage output V_{12}; at 500 kHz, V_{12} changes up to 5%; and at 1 MHz the variations are of up to 15% for R_x = 100 Ω, 150 Ω and 200 Ω.

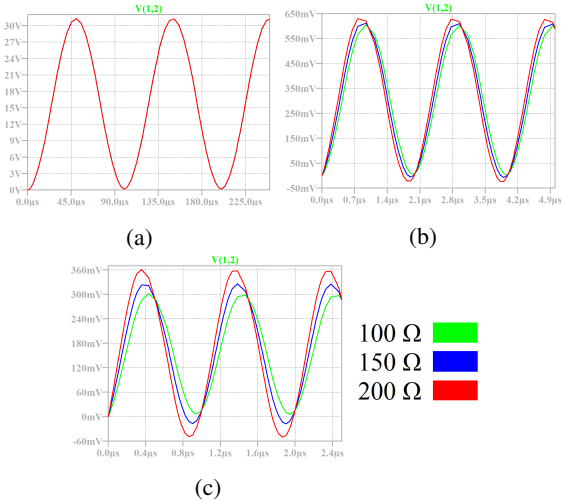

(a) (b)

(c)

Fig. 7: Simulation voltage output V_{12} as per Fig. 5a. This set of simulation voltages was obtained with $C = 1nF$. a) 10 kHz, b) 500 kHz c) 1 MHz.

2) Variable capacitance simulations: The second set of the Fig. 5b, gives the values of Table II. Irrespective of frequency, the ratio V_{12}/I_s cannot estimate correctly R_x. Note that the negative values observed in column 4 and column 8 at some frequencies are due to the phase difference between the detected voltage V_{12} and the injected current I_s. This phase shift is caused by the RC combination that is formed between the coupling capacitors (C_1, C_2, C_3, C_4) with the R_{13} and R_{24} resistors. This is true for both FSR402 and FSR406.

TABLE II: R_x simulation using two FSRs

FSR402				FSR406			
C_{13} C_{24} pF	f_c kHz	R_x Ω	V_{12}/I_s Ω	C_{13} C_{24} pF	f_c kHz	R_x Ω	V_{12}/I_s Ω
	10		495.0 k		10		197.0 k
	50		251.0 k		50		167.0 k
30	100	100	42.8 k	173	100	100	-16.2 k
	500		2.3 k		500		-819.0 k
	1000		-3.8 k		1000		-1.0 k

Table III shows the results of the same simulations as Table II except four FSRs are available instead of two. There is no shunt here and the value of R_x can be estimated from the V_{12}/I_s ratio, with an error of less than 4%. Therefore, using two FSRs as IPG electrodes is not possible even at a high 1 MHz frequency. Four FSRs on the contrary can give accurate bioimpedance variations in the range of 10 kHz to 1 MHz.

TABLE III: R_x simulation using four FSRs

FSR402				FSR406			
C_{13} C_{24} pF	f_c kHz	R_x Ω	V_{12}/I_s Ω	C_{13} C_{24} pF	f_c kHz	R_x Ω	V_{12}/I_s Ω
	10		98.3		10		98.3
	50		97.1		50		97.2
30	100	100	97.7	173	100	100	97.9
	500		96.8		500		96.7
	1000		96.8		1000		96.8

B. Experimental Plantar Impedance Plethysmography Signal

IPG allows to measure cardiac activity by bioimpedance variations: current is run through the tissue and voltage is measured between two intermediate points.

1) Impedance plethysmography with Ag-AgCl electrodes: Fig. 8 shows a cardiac signal of approximately 74 beats per minute (1.25 Hz during 60 s). Fig. 12 is the power spectrum of Fig. 8 obtained with the circuit of Fig. 6.

2) Impedance plethysmography with aluminum pads: Fig. 9 shows the signal acquired with Al-pads under the foot and inside the shoe. The cardiac rate is here 77 beats per minute (1.30 Hz during 60 s). Fig. 13 is the power spectrum of Fig. 9 of the same subject.

3) Impedance plethysmography with force sensors: Using four FSRs gets rid of the shunt resistors R_{13} and R_{24}, thus enabling IPG detection as shown in Fig. 10 and Fig. 11. The first IPG signal was obtained with G_1=50 and f_c=10 kHz while the second has a limited gain of G_1=5 with f_c=50 kHz.

Fig. 10 shows the results with four FSRs, using a carrier of 10 kHz, $G_1 = 50$. It is possible to detect the plantar IPG using FSRs as electrodes. The principal component of the cardiac activity can be seen in Fig. 14.

The same behavior was observed at 50 kHz, $G_1 = 5$, were the IPG signal is superimposed on a baseline drift. Fig. 15 shows the power spectral density of the ECG and the IPG

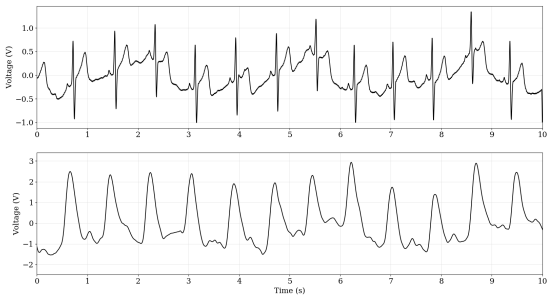

Fig. 8: Upper trace: Lead I ECG; lower trace: two Ag-AgCl 10 kHz IPG carrier - standing still subject ($G_1 = 3.5$).

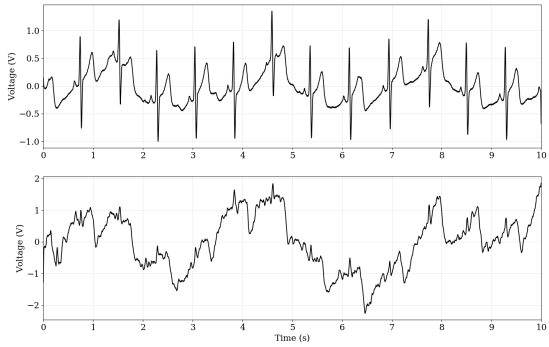

Fig. 9: Upper trace: Lead I ECG; lower trace: four Al-pads 10 kHz IPG carrier - standing still subject ($G_1 = 3.5$).

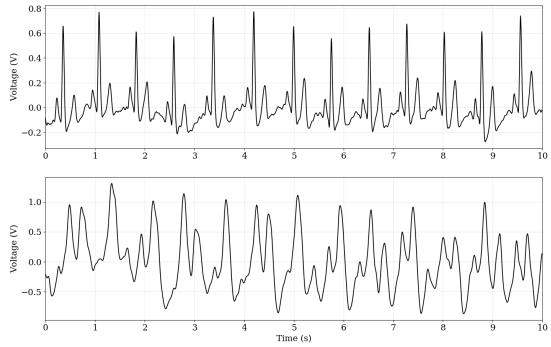

Fig. 10: Upper trace: Lead I ECG; lower trace: four FSRs 10 kHz IPG carrier - standing still subject ($G_1 = 50$).

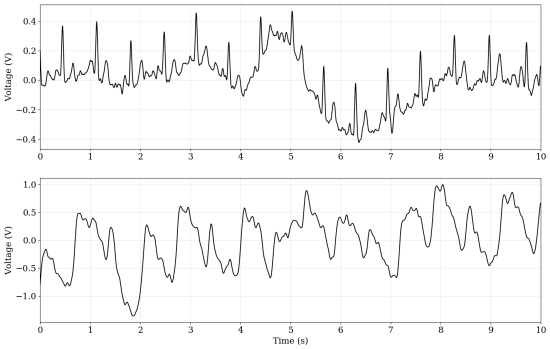

Fig. 11: Upper trace: Lead I ECG; lower trace: four FSRs 50 kHz IPG carrier - standing still subject ($G_1 = 5$).

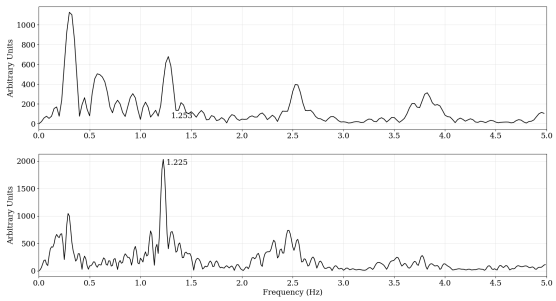

Fig. 12: FFT of lead I of the ECG (upper trace) and IPG obtained using a 10 kHz carrier and two Ag-AgCl electrodes (lower trace) of a standing still subject ($G_1 = 3.5$).

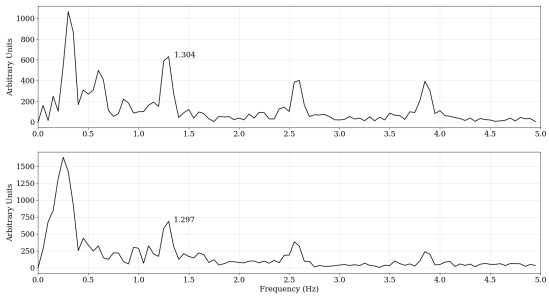

Fig. 13: FFT of lead I of the ECG (upper trace) and IPG obtained using a 10 kHz carrier and four Al-pads as electrodes (lower trace) of a standing still subject ($G_1 = 3.5$).

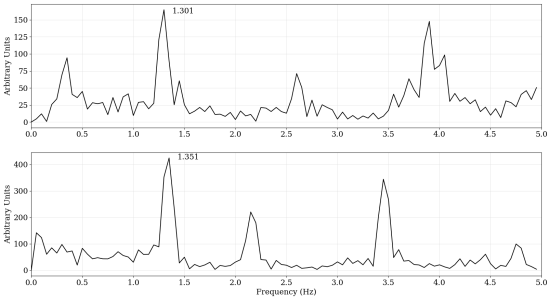

Fig. 14: FFT of lead I of the ECG (upper trace) and IPG obtained using 10 kHz and four FSRs as electrodes (lower trace) of a subject standing still ($G_1 = 50$).

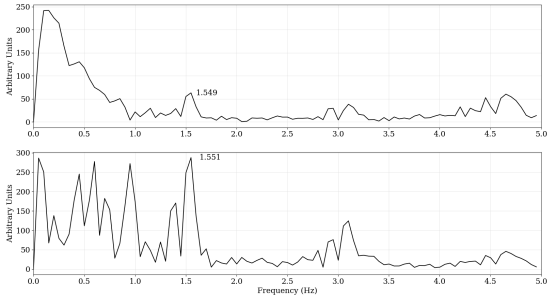

Fig. 15: FFT of lead I of the ECG (upper trace) and IPG obtained using a 50 kHz carrier and four FSRs as electrodes (lower trace) of a standing still subject ($G_1 = 5$).

signal of Fig. 11, where the heart rate component at 1.5 Hz is visible in both signals. In our experiment with the standing subject we could not detect the IPG signal at 100 kHz. This can be the consequence of using an IA of limited gain-bandwidth and a standard switch ADG436 to implement the synchronous demodulator

V. Discussion

As a feasibility study, we have explored the possibility of using FSR sensors simultaneously as pressure indicators and as bioimpedance electrodes. Using a validated model of these sensors, we have simulated their behavior at different frequencies, all compatible with bioimpedance measurements.

First, we have tested IPG and ECG simultaneous recordings with standard electrodes, namely AG-AgCl and Al-pads described in previous work [15]. Having obtained satisfactory IPG signals using conventional electrodes, we set ourselves the goal of substituting them with FSRs.

To check the viability of using FSRs as bioimpedance electrodes we presented at MeMeA 2021 [16] simulations at 10 kHz, 500 kHz and 1 MHz which showed us that at 1 MHz the circuit of Fig. 5a was able to give bioimpedance measurements as shown in Fig. 7. Specifically, Fig. 7c indicates that the simulated foot R_x resistance could be correctly measured at 50 Ω steps, between nodes 1 and 2 of Fig. 5a. At lower frequencies the bioimpedance measurement is not possible, since 50 Ω steps are not detected between nodes 1 and 2. We have nevertheless tried a real circuit (Fig. 2a) on a healthy subject at 10 kHz with no tangible results, as expected.

At 1 MHz the shunting resistors R_{13} and R_{24} have much higher impedance values than the foot bioimpedance seen by the two FSRs. But at 10 kHz, a frequency that stems from common electronic practice, no significant bioimpedance signal is detected between nodes 1 and 2.

The results obtained in 2021 [16] confirmed that FSRs can act as electrodes for bioimpedance measurements, which simplifies the development of a wearable device to alert patients of an imminent DFU. In the present report, simulation was extended to include specific capacitance values for the FSRs: 30 pF (FSR402), 173 pF (FSR406) and a foot bioimpedance of 100 Ω. The result shown in Table II led us to implement instead a four FSRs configuration as shown in Fig. 2b. The real measurement values on one side and the simulated values on the other side are within 4% as shown in Table III, which is a confirmation of agreement. Moreover, the ability to be used as bioimpedance electrodes is shared by FSR402 an FSR406 irrespective of the size of the contact area with the foot.

The important result derived from our simulations and experiments is that four FSRs are necessary to obtain IPG signals and simultaneous IPG and pressure signals. Using the four contacts of two FSRs appears to have no easy practical utility. This result enables us to plan multiplexed measurements of pressure and bioimpedance related variables such as IPG and foot composition.

Acceptable IPG signals are obtained using four FSRs at 10 kHz and 50 kHz, but the necessary gain is different, $G_1 = 50$ for 10 KHz and $G_1 = 5$ for 50 kHz. This information will be useful when designing the circuits to evaluate the diabetic foot prone to lesions.

We have confirmed that IPG activity is present in bioimpedance signals obtained from FSR406, provided we use two FSR per foot (Fig. 10 - Fig.14, Fig: 11 - Fig.15). The information obtained using FSRs is similar to that obtained using Al-pads (Fig. 9 - Fig.13).

The feasibility of measuring bioimpedance using sensors designed for other purposes is the main result of our work. Although IPG detection with different types of electrodes is commonplace, our work suggests a simultaneous (eventually multiplexed) recording of IPG and bioimpedance. Bioimpedance measurement can be readily obtained by averaging IPG signals. The use of several FSRs sensors could be implemented by time-multiplexing the sensors electrodes to yield different functions such as tissue composition estimation, cardiac activity and foot pressure.

One limitation of our work is related to the fact that two FSRs are not suitable for bioimpedance measurement and that four FSRs are instead necessary to obtain meaningful signals. One further limitation is that the measurement protocol included only a standing still subject, so as to rule out all possible motion artifacts.

We envisage to undertake simultaneous sensing of pressure and IPG during gait as a further step towards the design of a clinical device. Since our first objective was to verify the possibility of obtaining IPG and pressure simultaneously with FSRs, our results confirm that with appropriate time-multiplexing both signals are available from what we may call *multipurpose FSRs*. The hypothesis examined in this work consisted in determining the feasibility of sensor economy for a multi-variable instrument to continuously record foot variables of a person with diabetes. Therefore, it is important to use a single sensor for two purposes: plantar pressure and other parameters derived from the heart rate and the composition of foot tissues detected by bioimpedance. This encourages us to future work focused on measuring these parameters during gait.

Overall and despite all limitations, this paper paves the way to multiple use of FSR sensors.

VI. Conclusion

The present study shows the first results of a novel approach which consists of utilising standard FSR sensors also as bioimpedance electrodes. To test this capability of FSRs we have adopted, after circuit analysis and simulations, a system to detect the IPG signal using them in a tetra-polar arrangement. Configuration with 2 FSRs is not feasible to estimate impedance plethysmography but 4 FSRs show successful detection.

Acknowledgment

The authors would like to thank the Autonomous University of Ciudad Juárez for its research facilities. Additionally the authors would like to thank Beatriz Mendoza, MD, Professor and Head of the Metabolic Disorders and Diabetes Department, Universidad de la República, for insight and guidance

in the present research, as well as the members of her academic team. Therapist Karina Quinteros is also acknowledged here for practical clinical contributions to our work.

REFERENCES

[1] I. D. Federation, *International Diabetes Federation. Diabetes Atlas, 9th edn. Brussels, Belgium*, 2019. [Online]. Available: http://www.idf.org/sites/default/files/Atlas-poster-2014_ES.pdf

[2] N. C. Schaper, J. J. Van Netten, J. Apelqvist, S. A. Bus, R. J. Hinchliffe, and B. A. Lipsky, "Practical guidelines on the prevention and management of diabetic foot disease," International Working Group on the Diabetic Foot, IWGDF, Tech. Rep., 2019. [Online]. Available: https://iwgdfguidelines.org/wp-content/uploads/2019/05/01-IWGDF-practical-guidelines-2019.pdf

[3] S. A. Bus, "Innovations in plantar pressure and foot temperature measurements in diabetes," *Diabetes/Metabolism Research and Reviews*, vol. 32, pp. 221–226, 1 2016. [Online]. Available: http://doi.wiley.com/10.1002/dmrr.2760

[4] R. Vardasca, L. Vaz, C. Magalhaes, A. Seixas, and J. Mendes, "Towards the diabetic foot ulcers classification with infrared thermal images," *14th Quantitative InfraRed Thermography Conference*, pp. 1–4, 2018.

[5] S. L. Bennett, R. Goubran, and F. Knoefel, "Long term monitoring of a pressure ulcer risk patient using thermal images," *Proceedings of the Annual International Conference of the IEEE Engineering in Medicine and Biology Society, EMBS*, pp. 1461–1464, 2017.

[6] J. Kottner, J. Black, E. Call, A. Gefen, and N. Santamaria, "Microclimate: A critical review in the context of pressure ulcer prevention," *Clinical Biomechanics*, vol. 59, pp. 62–70, 2018. [Online]. Available: https://doi.org/10.1016/j.clinbiomech.2018.09.010

[7] J. M. Coates, "Podiatric skin health sensing in the diabetic foot," PhD Tesis, University of southampton, 2016.

[8] P. R. Cavanagh and J. S. Ulbrecht, "Clinical plantar pressure measurement in diabetes: rationale and methodology," *The Foot*, vol. 4, 1994.

[9] Ebers. (2021, 12) Sistema Ebers® . Accessed December 2021. [Online]. Available: https://ebersmed.com.ar/inicio

[10] N. DE. (2021, 12) Dynamic pressure distribution inside the footwear. Accessed December 2021. [Online]. Available: https://www.novel.de/products/pedar/

[11] C. Lou, S. Wang, T. Liang, C. Pang, L. Huang, M. Run, and X. Liu, "A graphene-based flexible pressure sensor with applications to plantar pressure measurement and gait analysis," *Materials*, vol. 10, 2017.

[12] L. A. Lavery, D. G. Armstrong, R. P. Wunderlich, J. Tredwell, and A. J. Boulton, "Predictive value of foot pressure assessment as part of a population-based diabetes disease management program," *Diabetes Care*, vol. 26, no. 4, pp. 1069–1073, 2003. [Online]. Available: https://care.diabetesjournals.org/content/26/4/1069

[13] A. Kekonen, M. Bergelin, M. Johansson, N. K. Joon, J. Bobacka, and J. Viik, "Bioimpedance sensor array for long-term monitoring of wound healing from beneath the primary dressings and controlled formation of h2o2 using low-intensity direct current," *Sensors*, vol. 19, 2019.

[14] D. H. Díaz, Óscar Casas, and R. Pallas-Areny, "Heart rate detection from single-foot plantar bioimpedance measurements in a weighing scale," in *2010 Annual International Conference of the IEEE Engineering in Medicine and Biology*, 2010, pp. 6489–6492.

[15] R. González-Landaeta, O. Casas, and R. Pallàs-Areny, "Heart rate detection from plantar bioimpedance measurements," *IEEE Transactions on Biomedical Engineering*, vol. 55, pp. 1163–1167, 2008.

[16] I. Morales, R. González-Landaeta, and F. Simini, "Pressure sensors used as bioimpedance plantar electrodes: a feasibility study," *16th IEEE International Symposium on Medical Measurements and Applications (MeMeA) Proceedings*, 2021.

[17] I. I. Electronics, "Fsr ® 400 series data sheet human," Interlink Electronics Inc. All Rights Reserved, Tech. Rep., 2015. [Online]. Available: www.interlinkelectronics.com

[18] D. Giovanelli and E. Farella, "Force sensing resistor and evaluation of technology for wearable body pressure sensing," *Journal of Sensors*, p. 13, 2016.

[19] P. Bertemes-Filho, "Electrical impedance spectroscopy," in *Bioimpedance in Biomedical Applications and Research*, F. Simini and P. Bertemes-Filho, Eds. Springer, 2018, pp. 5–28.

[20] P. S. Luna-Lozano and R. Pallàs-Areny, "Heart rate detection from impedance plethysmography based on concealed capacitive electrodes," *19th IMEKO World Congress 2009*, vol. 3, pp. 1766–1771, 2009.

[21] I. Morales, "Development of an electronic system for static and dynamic analysis of plantar pressure," Bachelor Tesis, Facultad de Informática y Electrónica, Universidad del Valle (Bolivia), 2011.

[22] A. Devices. (2020, 11) LTspice®. Accessed November 2020. [Online]. Available: https://www.analog.com/en/design-center/design-tools-and-calculators/ltspice-simulator.html

[23] R. Bragos, J. Rosell, and P. Riu, "A wide-band ac-coupled current source for electrical impedance tomography," *Physiological Measurement*, vol. 15, no. 2A, p. A91, 1994.

[24] *Monolithic Op Amp with Quad Low Noise AD844 Data Sheet*. [Online]. Available: https://www.analog.com/media/en/technical-documentation/data-sheets/AD844.pdf

[25] *High Speed FET-Input Instrumentation Amplifier INA111 Data Sheet*. [Online]. Available: https://www.ti.com/lit/ds/symlink/ina111.pdf

[26] R. Pallas-Areny and J. G. Webster, *Sensors and signal conditioning*. John Wiley and Sons, 2012.

[27] *Dual SPDT Switch ADG436 Data Sheet*. [Online]. Available: https://www.analog.com/media/en/technical-documentation/data-sheets/ADG436.pdf

[28] S. developers. (2020, 4) SciPy ecosystem. Accessed April 2020. [Online]. Available: https://www.scipy.org/about.html/

[29] I. Morales, R. González-Landaeta, and F. Simini, "Bioimpedance plethysmography with capacitive electrodes and sole force sensors: comparative trial," *Journal of Physics: Conference Series*, vol. 2008, no. 1, p. 012018, aug 2021. [Online]. Available: https://doi.org/10.1088/1742-6596/2008/1/012018

Isabel Morales is a Biomedical Engineer (Universidad del Valle, Bolivia) and Associate Professor of Biomedical Engineering at Núcleo de Ingeniería Biomédica (NIB) at Hospital de Clínicas, Universidad de la República, Uruguay since 2019, where she is working towards her PhD in Electrical Engineering.

Rafael González-Landaeta received the Engineer in Electronics degree in 1997 from the Rafael Belloso Chacín University, Maracaibo, Venezuela, and the Ph.D. degree in Biomedical Engineering in 2008 from the Universitat Politècnica de Catalunya, Barcelona, Spain. From 1999 to 2014, he has been an Associate Professor in Venezuela. Currently he is working in Biomedical Engineering at the Autonomous University of Ciudad Juarez, Mexico. From 2015 he is an Associate Editor of the Biomedical Engineering Mexican Journal. His current research areas include bioimpedance measurement, biomedical sensors and analog signal processing, noise and interference in electronic circuits, noninvasive physiological measurement, and energy harvesting.

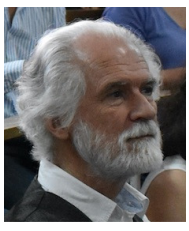

Franco Simini is Professor of Biomedical Engineering and Medical Informatics, Universidad de la República, Uruguay. He directs student projects and postgraduate theses, creates courses, publishes and holds patents. Biomedical instrumentation, Bioimpedance and Biomechanics are part of his research areas of interest.